Numerical Assessment of Microwave Imaging for Axillary Lymph Nodes Screening Using Anthropomorphic Phantom

Matteo Savazzi*, Jorge R. Costa†, Carlos A. Fernandes†, João M. Felício†, Raquel C. Conceição*
*Instituto de Biofísica e Engenharia Biomédica, Faculdade de Ciências, Universidade de Lisboa, 1749-016 Lisbon, Portugal, mlsavazzi@fc.ul.pt, rcconceicao@fc.ul.pt
†Instituto de Telecomunicações, Instituto Superior Técnico (IST), Universidade de Lisboa, 1049-001 Lisbon, Portugal, joao.felicio@lx.it.pt
‡Departamento de Ciências e Tecnologias da Informação, Instituto Universitário de Lisboa (ISCTE-IUL), Lisbon, Portugal
§Centro de Investigação Naval (CINAV), Escola Naval,Almada, Portugal

***Abstract*—We numerically assess the potential of microwave imaging (MWI) for the detection of axillary lymph nodes (ALNs). The proposed MWI system is radar-based, in which a broad-band signal (2-6 GHz) is transmitted by a single probing antenna to scan the axillary region. The full-wave simulations include a realistic phantom of the underarm region which was previously developed by the authors. The phantom includes the main tissues of the axillary region and the corresponding dielectric properties. We show that the proposed system can successfully detect an ALN embedded in a homogeneous fatty medium. Additionally, we show that despite the strong reflection of the muscle - caused by the high dielectric contrast between fat and muscle - we are able to distinguish an ALN from the background. To the best of our knowledge, this is the first study in literature which employs an anatomically realistic phantom to study ALN MWI.**

***Index Terms*—axillary lymph node imaging; broadband antenna, microwave imaging; numerical assessment; remote sensing.**

I. Introduction

Axillary Lymph Nodes (ALNs) are small, kidney-shaped organs of the lymphatic system, located in the underarm region. These organs are placed along the lymphatic vessels and they drain up to 75% of the lymph from the breasts. Due to their filtering role, ALNs are the first location where possible metastases from breast cancer tend to travel. For this reason, ALN diagnosis plays a crucial role in breast cancer patient therapy selection, and in the prognosis [1].

The state-of-the-art method for ALN diagnosis is the Sentinel Lymph Node Biopsy (SLNB), which consists of the surgical excision and histological examination of the first regional node (or nodes) to drain the primary tumour. However, SLNB is invasive and may lead to health complications, such as damage of blood vessels and nerves, incision infection, and lymphedema [2]. Clinical studies showed that more than 50% of early-stage invasive breast cancer patients have no ALN metastasis, meaning that SLNBs are unnecessary in those cases [3]. Therefore, it is clear that a non-surgical method of ALN diagnosis is needed. Alternatives include Magnetic Resonance Imaging (MRI) or the combination of Positron Emission Tomography and Computed Tomography (PET-CT), but their use is associated to high costs.

Microwave imaging (MWI) is a non-invasive and low-cost imaging modality, which has been studied for several application including breast cancer diagnosis [4], [5], [6] in the last two decades. More recently, our research group [7], [8], [9], [10] and other authors [11] proposed MWI as a possible means of ALN diagnosis. However, the research on ALN MWI is still in its initial stage, and such technique has not been tested on realistic models of the axillary region yet.

Here, we assess the viability of using microwaves to detect ALN through full-wave simulations, and we present the imaging results obtained from a radar system. The numerical setup includes an anthropomorphic phantom of the axillary region (previously described by the authors in [10]), which is scanned by a broadband antenna operating in the 2-6 GHz frequency-band. This application presents challenges that are not often posed by other MWI systems intended for biomedical applications. For instance, in breast and head MWI [12], [13], [14], the antennas are placed all around the body part, providing enough angular information to reconstruct the image. However, the morphology of the axillary region prevents such possibility, limiting the angular sweep of the antenna. In addition, the presence of the muscle tissue (which has very high dielectric properties) near the ALNs may hinder the sensing of the ALN response. As such, we first study the response of an ALN embedded in fat, suppressing the response of the muscle. As a second step, we focus on the impact of the muscle on the imaging results. To this end, we consider also the muscle response when reconstructing the image of the phantom. In the latter case, despite the degradation of the ALN response, we still manage to detect the ALN. To the best of our knowledge this is the first time in literature that an axillary MWI setup is studied with a realistic phantom.

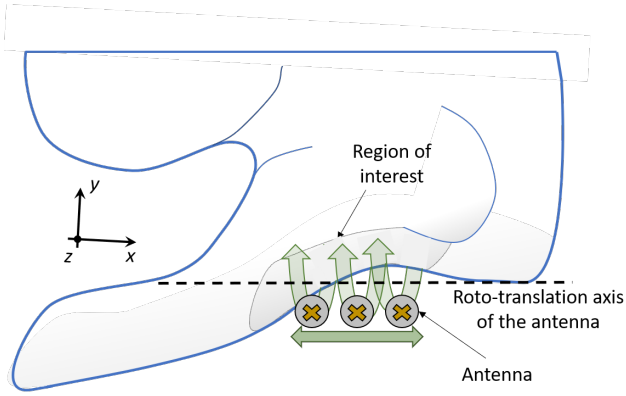

Fig. 1. Axillary microwave imaging setup (taken from [10]): the patient lays in a supine position while the antenna roto-translates along the z-axis, scanning the axillary region. In a - more realistic - clinical scenario, we may consider a bed with an opening where the patient can insert her arm. This would allow easy access to the axillary region, while ensuring the patient is stable.

II. Microwave Imaging Setup

In this section we describe the MWI setup, together with the anatomically and dielectrically realistic phantom representative of the female axillary region, which serves to test the application of MWI to detect ALNs.

In order to scan the axillary region, we designed our setup considering a scenario in which the patient lays in a supine position, with her arm extended along the head. The setup is a radar-type, monostatic system, which employs a single antenna roto-translating around the axillary region. We opted for a monostatic system for its simplicity as studies of the axillary MWI are still at their initial stage. A schematic of the setup is reported in Fig. 1. We note that, in contrast with most MWI prototypes, our setup does not require an immersion liquid, which represents an advantage both in terms of system design and patient hygiene. The feasibility of a dry setup was assessed in [12], where the authors quantified - for the case of breast MWI - the reduction of skin reflection caused by different matching media. In that study, the authors concluded that the adoption of an immersion liquid can mitigate the reflection by 8 dB at maximum (1-6 GHz bandwidth). If we consider the expected response of an ALN (-60 dB to -70 dB according to [10]) and the dynamic range of our VNA (110dB), we can conclude that an 8 dB power reduction due to skin backscattering is manageable and, therefore, does not preclude a dry imaging setup for ALN MWI.

The probing antenna consists of a cross-Exponentially Tapered Slot (XETS) antenna, operating in the 2-6 GHz frequency band, which was proposed in [15]. The XETS is well suited for imaging applications not only for its impedance matching over a broad bandwidth but also because it presents a stable phase centre along the frequency. In this study, we sampled the antenna reflection coefficient in 667 equally-spaced frequency points, covering the whole operating bandwidth of the XETS.

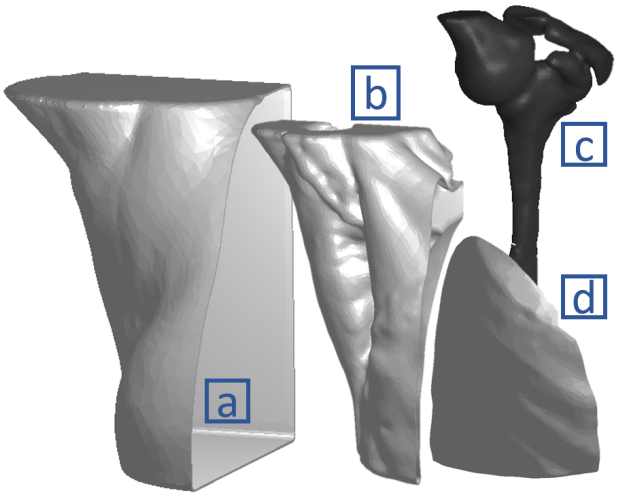

(a)

Fig. 2. Numerical model of the phantom axillary organs used to test the application of axillary lymph node microwave imaging. (a) fat container; (b) muscle container; (c) bone; (d) lung container. Note that the outer container (i.e. fat container) is open on one side, in order to contain the other organs. The muscle and lung containers are designed with an aperture to allow filling them with appropriate tissue mimicking liquids. As for the bone, this is a 3D-printed fully solid part.

Regarding the axillary model, we used the numerical model of the 3D-printed anthropomorphic phantom, which we recently proposed in [10]. The phantom is derived from the segmentation of a thoracic CT scan, and it includes five tissues of interest for realistic representation of the axillary region given the intended application: fat, muscle, bone, lung, and ALNs. Except for the bone and the ALN organs (made of solid tissue-mimicking materials), fat, muscle, and lung are polymeric cavities, which can be filled with appropriate tissue-mimicking liquids. Fig. 2 shows the numerical model of the organ containers, which we used for the numerical test of our MWI system. For the purpose of our study, we included one spherical ALN (radius = 5mm) to the above described axillary model. The ALN is embedded in fat tissue, and spaced 5mm from the phantom-air interface.

Regarding tissue dielectric properties, we assigned their values for fat, muscle, lung, and bone according to [16]; while we used the dielectric properties that we recently measured in [10] for the ALN. As for the phantom containers, these have dielectric constant of 2.5 and a loss tangent of 0.02.

III. Numerical Assessment

This section describes the signal processing and presents the imaging results obtained from full-wave simulations - using Computer Simulation Technology (CST) Microwave transient solver [17].

A. Signal processing

We applied an image reconstruction algorithm based on the wave migration proposed in [18]. The intensity I of each

image voxel is computed as follows:

$$I(v) = \sum_{i}^{N_{ant}} \sum_{f_k}^{N_f} s_{ii}(f_k) e^{jk_0(2d_{air}+2d_{fat}n_{fat})} \quad (1)$$

where d_{air} is the distance between the XETS antenna and the phantom surface, d_{fat} is the distance between the voxel and the phantom surface, and n_{fat} is the refractive index of fat. S_{ii} is the (calibrated) reflection coefficient measured for the i^{th} antenna position which has 1xN_f size, where N_f is the number of frequency points. N_{ant} is the number of antenna positions. $k_0 = \frac{2\pi f_k}{c}$ is the wave-number in vacuum, where c is the speed of light in vacuum.

We note that the presented algorithm does not consider a proper wavenumber for the propagation inside the muscle tissue. This is justified by the fact that the ALNs we aim to image are embedded only in fat, and lay between skin and muscle. For this reason, we did not consider the accurate reconstruction the muscle region.

B. Imaging results

We defined a total of 10 antenna positions, spaced by a 6° angular step on a circular trajectory which lies down on the same XY-plane (reference system in Fig. 1) of the ALN. The sweep radius is 85mm, resulting in a 9mm distance between adjacent antenna positions. The distance between the antenna and the phantom surface ranges between 20mm and 30mm, depending on the antenna position.

Fig. 3 shows the obtained reconstructed image in the XY-plane which contains the ALN. We note that, to reconstruct the image in Fig. 3a, we input in (1) a reflection coefficient (S_{ii}) computed as the difference between the reflection coefficient obtained when illuminating the axillary phantom with all its components (polymeric containers, fat, muscle, lung, and ALN) and the reflection coefficient obtained when illuminating the same setup without the ALN (target). This operation can be interpreted as an approximation to a "S_{ii} calibration" which allows us to isolate the response of the ALN.

The resulting image in Fig. 3a shows that we can successfully detect an ALN in its correct location when isolating the response of the ALN. The overall size of the detected ALN is slightly larger than the physical dimension of the ALN that was considered in the simulation. This is a consequence of the limited angular positions that we can use to probe the axillary region. Nevertheless, the ALN is detected at its correct coordinates.

In order to study the influence of the muscle on the imaging results, we reconstructed a similar numerical setup, but at this time we intentionally kept both the response of the ALN and the muscle. To do so, we input in (1) an S_{ii} which was computed as the difference between the reflection coefficient obtained from all the axillary phantom components and the simulated reflection coefficient from the same setup without ALN and muscle. By focusing both on the ALN and muscle responses, we can study the impact of the muscle on the imaging results. The results are shown in Fig. 3b.

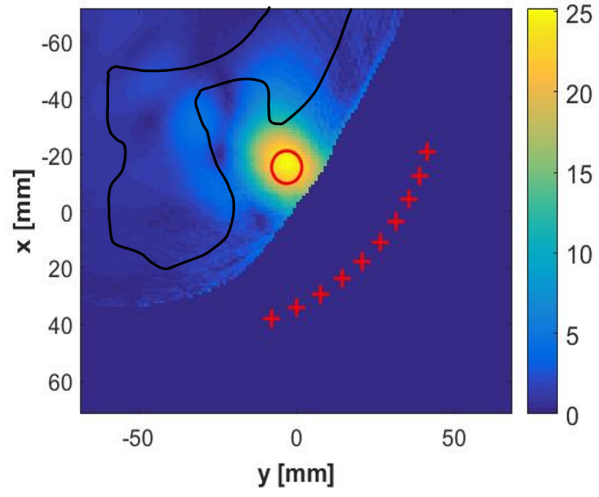

(a)

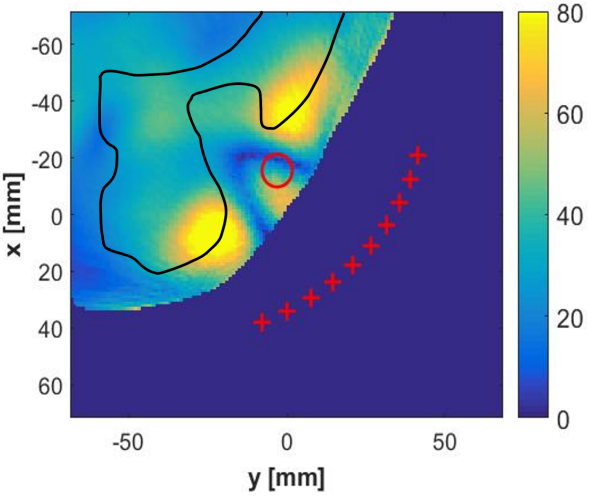

(b)

Fig. 3. Reconstructed energy map of the axillary region with one axillary lymph node (ALN). The represented XY-plane corresponds to the one which cuts the ALN center. The red crosses indicate the antenna positions; the inner red circle shows the actual position of the ALN; the black line traces the profile of the muscle. In **(a)** the reflection coefficient (S_{ii}) is calibrated to isolate the ALN response; while in **(b)** the S_{ii} is calibrated to isolate the ALN and the muscle responses.

Compared to Fig. 3a, there is an obvious deterioration of the imaging results, as a consequence of the large dielectric contrast between the muscle and the fat. Moreover, there is a kind of symmetric response due to the muscle. In between the two highest magnitude points in the image, we were able to detect the ALN. We consider this a promising result given the large surface of the muscle and its dielectric properties, compared to the ALN.

The next step of this work is to study more ALN positions around the muscle, so to evaluate the extent of the impact of the muscle on the detection of the ALN.

IV. Conclusions and future work

We numerically assessed the feasibility of a MWI system for ALN detection using - for the first time in literature - an anatomically realistic phantom of the axillary region.

Despite the challenges posed by the limited angular sweep of the antenna, we showed that our system can detect a 5mm radius ALN embedded in fat. In addition, we showed that, when taking into account the strong reflection of the nearby muscle tissue, the ALN can still be detected.

These results are encouraging to proceed with the investigation of MWI for ALN detection. In the future, we plan to extend the study to more complex cases, which will include several ALNs, with different sizes, shapes, and positions. Moreover, we aim to remove the muscle response, by using a data-adaptive algorithm that we previously used as artifact removal to mitigate the skin response.

Acknowledgment

This work was supported by the EMERALD project funded from the European Union's Horizon 2020 research and innovation programme under the Marie Skłodowska-Curie grant agreement No. 764479.

This work is also supported by Fundação para a Ciência e a Tecnologia-FCT, FCT/MEC (PIDDAC) under the Strategic Programme UID/BIO/00645/2020, and UIDB/50008/2020.

References

[1] G. H. Lyman, A. E. Giuliano, M. R. Somerfield, A. B. Benson III, D. C. Bodurka, H. J. Burstein, A. J. Cochran, H. S. Cody III, S. B. Edge, S. Galper *et al.*, "American Society of Clinical Oncology Guideline Recommendations for Sentinel Lymph Node Biopsy in Early-Stage Breast Cancer," *Journal of Clinical Oncology*, vol. 23, no. 30, pp. 7703–7720, 2005.

[2] G. H. Lyman, M. R. Somerfield, L. D. Bosserman, C. L. Perkins, D. L. Weaver, and A. E. Giuliano, "Sentinel Lymph Node Biopsy for Patients with Early-Stage Breast Cancer: American Society of Clinical Oncology Clinical Practice Guideline Update," *Journal of Clinical Oncology*, vol. 35, no. 5, pp. 561–564, 2017.

[3] L. Ouldamer, F. Arbion, A. Balagny, F. Fourquet, H. Marret, and G. Body, "Validation of a Breast Cancer Nomogram for Predicting Nonsentinel Node Metastases After Minimal Sentinel Node Involvement: Validation of the Helsinki Breast Nomogram," *The Breast Journal*, vol. 22, no. 5, pp. 787–792, 2013.

[4] S. C. Hagness, A. Taflove, and J. E. Bridges, "Two-Dimensional FDTD Analysis of a Pulsed Microwave Confocal System for Breast Cancer Detection: Fixed-Focus and Antenna-Array Sensors," *IEEE Transactions on Biomedical Engineering*, vol. 45, no. 12, pp. 1470–1479, 1998.

[5] Y. Xie, B. Guo, L. Xu, J. Li, and P. Stoica, "Multistatic Adaptive Microwave Imaging for Early Breast Cancer Detection," *IEEE Transactions on Biomedical Engineering*, vol. 53, no. 8, pp. 1647–1657, 2006.

[6] R. C. Conceição, J. J. Mohr, and M. O'Halloran, *An Introduction to Microwave Imaging for Breast Cancer Detection*. Springer, 2016.

[7] R. Eleutério, A. Medina, and R. C. Conceição, "Initial Study with Microwave Imaging of the Axilla to Aid Breast Cancer Diagnosis," in *2014 USNC-URSI Radio Science Meeting (Joint with AP- Symposium), Memphis, TN, USA,*. IEEE, 2014, pp. 306–306.

[8] D. M. Godinho, J. M. Felício, T. Castela, N. A. Silva, M. L. Orvalho, C. A. Fernandes, and R. C. Conceição, "Extracting Dielectric Properties for MRI-Based Phantoms for Axillary Microwave Imaging Device," in *2020 14th European Conference on Antennas and Propagation (EuCAP), Copenaghen, Denmark*. IEEE, 2020, pp. 1–4.

[9] M. Savazzi, E. Porter, M. O'Halloran, J. R. Costa, C. Fernandes, J. M. Felicío, and R. C. Conceição, "Development of a Transmission-Based Open-Ended Coaxial-Probe Suitable for Axillary Lymph Node Dielectric Measurements," in *2020 14th European Conference on Antennas and Propagation (EuCAP), Copenaghen, Denmark*. IEEE, 2020, pp. 1–5.

[10] M. Savazzi, S. Abedi, N. Ištuk, N. Joachimowicz, H. Roussel, E. Porter, M. O'Halloran, J. R. Costa, C. A. Fernandes, J. M. Felício *et al.*, "Development of an Anthropomorphic Phantom of the Axillary Region for Microwave Imaging Assessment," *Sensors (Basel, Switzerland)*, vol. 20, no. 17, pp. 49–68, 2020.

[11] J. Liu and S. G. Hay, "Prospects for Microwave imaging of the Lymphatic System in the Axillary," in *2016 IEEE-APS Topical Conference on Antennas and Propagation in Wireless Communications (APWC), Cairns, QLD, Australia*. IEEE, 2016, pp. 183–186.

[12] J. M. Felício, J. M. Bioucas-Dias, J. R. Costa, and C. A. Fernandes, "Microwave Breast Imaging Using a Dry Setup," *IEEE Transactions on Computational Imaging*, vol. 6, pp. 167–180, 2020.

[13] B. L. Oliveira, D. O'Loughlin, M. O'Halloran, E. Porter, M. Glavin, and E. Jones, "Microwave Breast Imaging: Experimental Tumour Phantoms for the Evaluation of New Breast Cancer Diagnosis Systems," *Biomedical Physics & Engineering Express*, vol. 4, no. 2, p. 025036, 2018.

[14] O. Karadima, M. Rahman, I. Sotiriou, N. Ghavami, P. Lu, S. Ahsan, and P. Kosmas, "Experimental Validation of Microwave Tomography with the DBIM-TwIST Algorithm for Brain Stroke Detection and Classification," *Sensors*, vol. 20, no. 3, p. 840, 2020.

[15] J. R. Costa and C. A. Fernandes, "Broadband Slot Feed for Integrated Lens Antennas," *IEEE Antennas and Wireless Propagation Letters*, vol. 6, pp. 396–400, 2007.

[16] S. Gabriel, R. Lau, and C. Gabriel, "The Dielectric Properties of Biological Tissues: II. Measurements in the Frequency Range 10 Hz to 20 GHz," *Physics in Medicine & Biology*, vol. 41, no. 11, p. 2251, 1996.

[17] "Cst Studio Suite," https://www.3ds.com/products-services/simulia/products/ cst-studio-suite/, accessed on 26/02/2020.

[18] J. M. Lopez-Sanchez and J. Fortuny-Guasch, "3-D Radar Imaging Using Range Migration Techniques," *IEEE Transactions on antennas and propagation*, vol. 48, no. 5, pp. 728–737, 2000.